

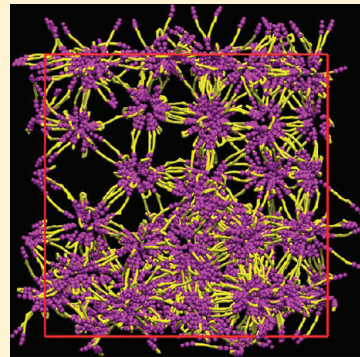
Nanoscale Organization in Aqueous Dicationic Ionic Liquid Solutions

B. L. Bhargava*†,‡ and Michael L. Klein†

*Institute for Computational Molecular Science and Department of Chemistry, Temple University, 1900 N. 12th Street, Philadelphia, Pennsylvania 19122, United States

†The Laboratory for Research on the Structure of Matter, University of Pennsylvania, 3231 Walnut Street, Philadelphia, Pennsylvania 19104-6202, United States

ABSTRACT: Coarse-grained molecular dynamics simulations have been performed on aqueous solutions of the gemini dicationic ionic liquid 1,5-bis(3-decylimidazolium-1-yl) pentane bromide at room temperature to study the structure and organization in the solution. Several trajectories corresponding to different concentrations of the ionic liquid (IL) in the solution were generated for about a microsecond. The 40% (w/w) aqueous mixture evolves to a hexagonal structure starting from a random distribution of ions. Spontaneous aggregation of cations was observed in solutions at lower concentrations. Unlike the monocationic ILs, which form spherical aggregates, the aggregates observed in the dicationic IL solution displayed a near-hexagonal arrangement of the hydrophobic cores that were connected to each other by hydrophilic head groups. Anions were found to be present close to the polar head groups. The formation of the interlinked aggregates from a random distribution and the organization at the vapor–liquid interface are also discussed.



1. INTRODUCTION

Aqueous solutions of room-temperature ionic liquids (RTILs) have generated considerable interest among researchers recently.^{1–5} ILs with short alkyl tails are isotropic in their neat form and have been studied using various experimental techniques^{6–8} and computational studies.^{9–12} The long-alkyl-chain-substituted imidazolium-based ionic liquids (ILs) exhibit distinct phases as the water content in their mixture with water is changed.^{13–16} These phases are a result of the presence of polar and nonpolar regions, where the polar region of the cations, anions, and water molecules form a hydrogen-bonded network and the nonpolar regions are segregated from the polar region. At lower concentrations of the IL, above the critical aggregation concentration (CAC), the amphiphilic nature of the cations leads to the aggregation of cations forming “spherical” micelles, with the aggregation number increasing with concentration.¹⁶

Imidazolium cationic ILs ($[C_n\text{mim}][\text{Br}]$) with short alkyl chains ($n = 2–6$) do not form definite aggregates, but those with longer tails ($n > 8$) form well-defined aggregates.^{17–21} The aggregation and critical micelle concentration (CMC) of these systems have been studied using several experimental techniques.^{22,23} The structure of the aggregates and mesophase behavior of high-concentration mixtures have been studied using atomistic and coarse-grained molecular dynamics (MD) simulations.^{24–27} The aqueous solutions of long-alkyl-chain-substituted ILs can be used as surfactants because of their amphiphilic nature. Recently, a new category of ILs with multiple charge centers has begun to receive attention.^{28–36}

Geminal dicationic ILs with two charge centers are composed of two singly charged cations linked to each other by a spacer, which is usually an alkyl chain. In their crystalline phase, a singly charged anion is associated with each charge center. Geminal dicationic ILs have been synthesized and characterized^{28–33}

recently and have also been used in chemical reactions.^{34–36} Dicationic imidazolium bromide IL with a tetradecyl chain is known to exhibit a higher thermal stability and a significantly lower CMC (by 2 orders of magnitude) than its monocationic IL counterpart with the same length of alkyl chain.³⁰ Gemini surfactants with multiple polar and nonpolar regions are known to form complex aggregate structures.³⁷ Previous experimental and computational studies^{37–39} on gemini surfactant solutions have reported the formation of threadlike and treelike micelles depending on the length, flexibility, and hydrophobicity of the spacer. In addition to their usability as surfactants because of their amphiphilicity, dicationic ILs can also be used as solvents and lubricants owing to their high thermal stability.⁴⁰ They are also used in gas chromatography columns (as the stationary phase),⁴¹ in electrospray ionization mass spectrometry, and in the detection of small quantities of anions by gas-phase ion association.⁴²

Dicationic ILs have received little attention of researchers compared to monocationic ILs, with few experimental and computational studies reported so far.^{43–45} Molecular dynamics (MD) studies⁴⁵ using fully atomistic simulations are of limited capability to explore the complex equilibrium structures of aqueous solutions of dicationic ILs at the nanoscale level because of the requirement of large computational resources. To overcome these limitations, we have developed a coarse-grained (CG) model for aqueous solution of 1,5-bis(5-decylimidazolium-1-yl) pentane bromide $\{[C_5(C_{10}\text{Im})_2] \cdot 2\text{Br}\}$, in which two 1-*n*-decylimidazolium units are linked by a $-(C_5\text{H}_{10})-$ group at 3-position $\}$ and performed CG-MD simulations at various concentrations of the

Received: May 11, 2011

Revised: July 27, 2011

Published: July 28, 2011

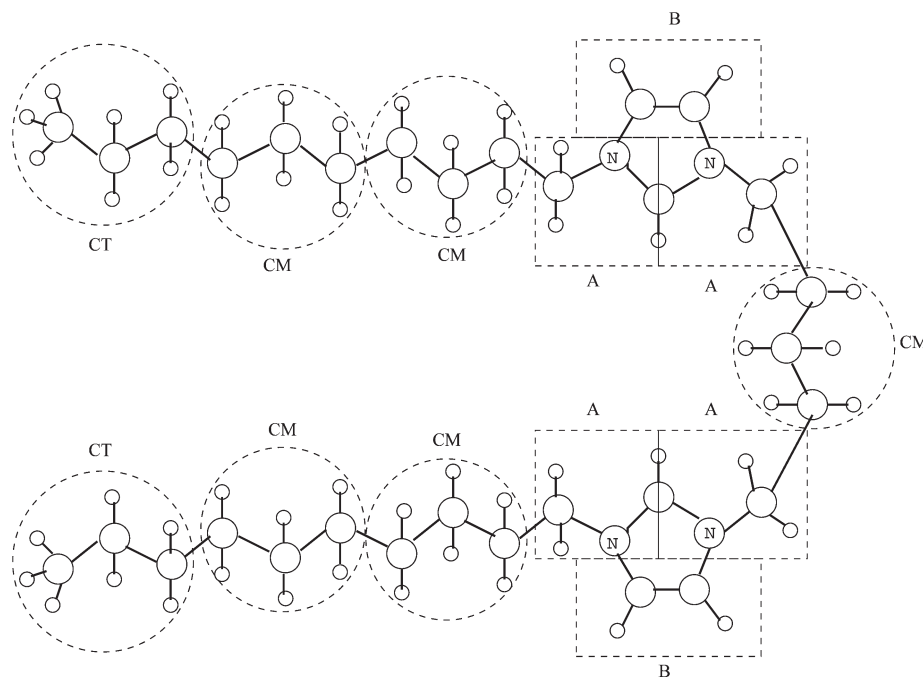


Figure 1. Schematic of the $[C_5(C_{10}Im)_2]$ cation illustrating the mapping of atoms to coarse-grained beads: CT, CM, A, and B.

water–IL binary system. Herein, we provide details of the MD simulations, followed by a presentation of the results and related discussion. We end with the conclusions drawn from the reported computational studies.

2. METHODOLOGY AND SIMULATION DETAILS

The mapping of atoms into CG beads is presented as a schematic in Figure 1. The CG representation in the current studies is similar to that employed in our previous work,^{46,47} in which a bead typically represents three non-hydrogen atoms and their associated hydrogens. The imidazolium ring along with the attached methylene groups is represented using three beads so as to retain its planar nature. Each nonyl chain is represented by three beads, and the central spacer is represented by a single bead. Thus, in total, the 93 atoms of the cation are mapped into 13 beads. Because the size of the bromide ion is comparable to the size of other beads, it is represented by a unique bead. Three water molecules are modeled as a single CG site in accordance with the Shinoda et al. model.⁴⁸ The charges on the beads were obtained by summing the atomic partial charges and then scaling them to 0.25 of the total. The positive charge was concentrated on the three beads forming the imidazolium ring, whereas the remaining beads representing the alkyl chains and water were neutral. The mass of each bead was obtained by summing the masses of constituent atoms. The initial configuration of the system was obtained from a well-equilibrated all-atom system by the mass weighted atom coordinates. The cation thus has four types of beads: CT, CM, A, and B.

The beads interact with each other through bonded and nonbonded interactions. The intramolecular interactions, which are applicable to only cations by construct, include bond stretching and bending interactions. The intramolecular interaction parameters were derived from the distributions computed from all-atom (AA) MD simulations.⁴⁶ The form of the intramolecular potential

used in the simulations is

$$U_{\text{intra}} = \sum_{\text{bonds}} k_b(r - r_0)^2 + \sum_{\text{angles}} k_\theta(\theta - \theta_0)^2 \quad (1)$$

where k_b and k_θ are force constants and r_0 and θ_0 are the equilibrium bond length and bond angle, respectively. The intramolecular parameters used in these simulations can be found elsewhere.⁴⁶

Coulomb and dispersion interactions constitute the nonbonded interactions between the beads. Beads within a molecule also interacted through nonbonded interactions if they were separated by more than two bonds. Dispersion interactions were handled using either a 9–6 or a 12–4 Lennard–Jones (L–J) potential. Pair interactions not involving water beads were handled with a 9–6-type L–J interaction given by

$$U_{\text{LJ}9-6} = \frac{27}{4} \varepsilon \left[\left(\frac{\sigma}{r} \right)^9 - \left(\frac{\sigma}{r} \right)^6 \right] \quad (2)$$

For pairs in which at least one of the beads is water, a 12–4-type L–J potential was used to handle the dispersion interaction, given by

$$U_{\text{LJ}12-4} = \frac{3\sqrt{3}}{2} \varepsilon \left[\left(\frac{\sigma}{r} \right)^{12} - \left(\frac{\sigma}{r} \right)^4 \right] \quad (3)$$

where ε is the minimum energy and σ is the distance at which the L–J interaction energy is zero.

The charges on the cations and anions were reduced to +0.25 and –0.25 e, respectively. The three beads constituting the ring carried charges of 0.105, 0.105, and 0.040 e. To compensate for the absence of polarization due to the use of coarse water beads, the charge had to be scaled down. Nonbonded interaction parameters were assigned and refined so as to reproduce the all-atom pair distribution functions. Final values of the L–J

Table 1. Lennard-Jones Interaction Parameters

bead pair	ϵ (kcal mol ⁻¹)	σ (Å)	bead pair	ϵ (kcal mol ⁻¹)	σ (Å)
A–A	0.1000	5.2000	CM–CM	0.4200	4.5060
A–B	0.1000	5.2000	CM–CT	0.4440	4.5455
A–CM	0.1200	4.8000	CM–Br	0.0800	5.1000
A–CT	0.1500	4.4000	CM–W	0.3400	4.4385
A–Br	0.0600	4.8000	CT–CT	0.4690	4.5850
A–W	0.4000	3.8500	CT–Br	0.1000	5.2000
B–B	0.0500	4.7500	CT–W	0.3600	4.4780
B–CM	0.1300	3.7600	Br–Br	2.0000	4.0000
B–CT	0.2600	3.9000	Br–W	0.8950	3.9000
B–Br	0.0500	4.3000	W–W	0.8950	4.3710
B–W	0.4000	3.6500			

Table 2. Details of Simulations Performed

system	no. of cations	no. of water beads	box dimensions (nm)	run length (μs)
Bulk-I	3375	26920	18.03, 18.03, 18.03	1.0
Bulk-II	1000	29888	15.40, 15.40, 15.40	1.0
Bulk-III	540	40500	16.09, 16.09, 16.09	1.0
Bulk-IV	400	80000	19.65, 19.65, 19.65	1.0
Interface	1000	29888	15.40, 15.40, 24.00	1.0

interaction parameters used in the simulations are listed in Table 1. The details of the AA-MD simulations can be found elsewhere.⁴⁵

A real-space cutoff distance of 15 Å was employed for the nonbonded interactions, and the potential was not shifted at the cutoff. The interaction parameters from the Shinoda et al. model⁴⁸ were retained for the alkyl chain beads and water beads. The geometry of the molecule was used in determining the initial values of σ for the beads, which were then refined to obtain pair correlation functions comparable with those from the corresponding AA MD data.

The CG model was used to simulate several aqueous [C₅(C₁₀Im)₂]·2Br solutions at various concentrations. Table 2 provides the details of the simulations performed. For every cation, two bromide anions were included to neutralize the solution.

Simulations were performed at room temperature (300 K) and atmospheric pressure using the MD package LAMMPS.⁴⁹ The density of the system was fixed from initial simulations that were carried out in the isothermal–isobaric ensemble (i.e., constant NPT). Subsequent simulations were performed in the canonical ensemble (i.e., constant NVT). The multiple-time-step algorithm rRESPA⁵⁰ was used to integrate the equations of motion, wherein the bonded interactions and nonbonded interactions were computed every 3 and 6 fs, respectively. Nosé–Hoover thermo- and barostats with time constants of 100.0 and 1000.0 fs, respectively, were used to control the temperature and pressure of the system. A particle–particle particle-mesh (PPPM) solver with an accuracy of 1.0×10^{-6} was used to handle Coulombic interactions.

The initial configuration for the system used in refining the nonbonded interaction parameters was obtained from an equilibrated configuration from an AA MD simulation consisting of 125 cations, 250 anions, and 11208 water molecules. With the final refined interaction parameters, this system was further

equilibrated and replicated twice along each of the Cartesian coordinate axes to obtain a system with 1000 cations, 2000 anions, and 26920 water beads (Bulk-II). This system was further equilibrated and was placed in the center of a supercell of dimensions 15.40, 15.40, and 24.00 nm to construct the interfacial system (Interface). The system Bulk-I was obtained by a 3-fold replication of the initial system along each of the axes and removal of the water molecules randomly. Systems Bulk-III and Bulk-IV were constructed by replicating the initial system three times along all of the axes and randomly removing ion pairs and water molecules. The visualization software VMD⁵¹ was used to render images.

3. RESULTS AND DISCUSSION

3.1. Structure Factor. Partial radial distribution functions (RDFs) were computed for all distinct pairs of bead types, with a bin width of 0.05 Å, up to a distance equal to one-half of the box length. Partial structure factors were calculated between all distinct pairs of beads using the formula

$$S_{\alpha\beta}(q) = \delta_{\alpha\beta} + 4\pi\sqrt{\rho_\alpha\rho_\beta}\int_0^\infty r^2[g_{\alpha\beta}(r) - 1]\frac{\sin(qr)}{qr} dr \quad (4)$$

where $\rho_\alpha = N_\alpha/V$, N_α is the number of beads of type α , V is the volume of the system, $g_{\alpha\beta}(r)$ is the radial distribution function between pairs of types α and β , and δ is the Kronecker delta function. The upper limit of the integral was taken as one-half of the length of the cubic simulation box. The total X-ray structure factor is given by

$$S(q) = \sum_\alpha \sum_\beta c_\alpha c_\beta \frac{f_\alpha(q) f_\beta(q)}{\langle f(q) \rangle^2} S_{\alpha\beta}(q) \quad (5)$$

where c_α is the concentration of bead type α , f_α is the form factor of bead α , and $\langle f(q) \rangle = \sum_\alpha c_\alpha f_\alpha(q)$.

The length of the cubic box determines the resolution of the q value in the simulations. In the present studies, the minimum value of q for the Bulk-I mixture was 0.0348 Å⁻¹. The RDFs used in the calculation of structure factors were averaged over the last 60 ns of each trajectory. In CG-MD simulations, comparison with experiments can be made only beyond certain length scale, as the atomistic details are lost during coarse graining. Thus, the results are comparable up to a q value of around 2 Å⁻¹. The form factors of the constituent atoms were summed to obtain the X-ray form factors for the beads.

The computed X-ray structure factor for the Bulk-I mixture [40% (w/w) water] is shown in Figure 2. The inset of the figure also shows the medium-range correlation observed at the q value of 1.58 Å⁻¹ corresponding to a length scale of about 4 Å. We observed a very strong peak at the wave vector of 0.19 Å⁻¹. This can be compared with the experimentally observed¹⁴ peak at 0.189 Å⁻¹ for the 40% (w/w) water mixture of [C₁₀mim][Br], which also has a decyl chain. The peak in the structure factor corresponds to a spatial correlation present at a real-space separation of 33 Å. The mesophase structure observed is discussed later in this article. Even though a small peak can be seen at very low wave vector, the statistical noise at that end precludes any meaningful assertions about it. Analysis of the partial structure factor between pairs suggests that the main contribution to the peak at 0.19 Å⁻¹ comes from the correlation between the

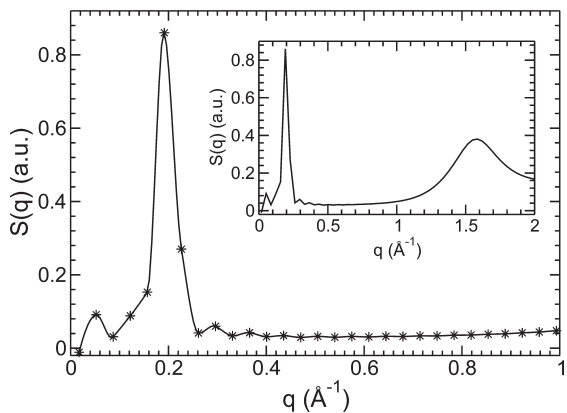


Figure 2. X-ray structure factor computed from the CG-MD trajectory for the 40% (w/w) water mixture showing the low-wave vector region. Akima interpolation was used to smooth the data. Inset: Structure factor up to a wave vector of 2\AA^{-1} .

tail beads (i.e., CT–CT, CT–CM, and CM–CM, with CM bonded to CT).

3.2. Structural Organization in the Mixture. Long-chain ILs are known to exhibit different mesophase structures upon addition of water. For example, ionogels of $[\text{C}_{10}\text{mim}][\text{Br}]$ with 11–16% (w/w) water have a lamellar structure, which undergoes a transition to a hexagonal perforated layered structure at 17% (w/w) water. Upon further dilution to around 40% (w/w) water, the mixture converts to a low-viscosity hexagonal phase.¹⁴ Formation of the hexagonal columnar phase from a random configuration in a 37% (w/w) water mixture of $[\text{C}_{10}\text{mim}][\text{Br}]$ was also observed in computational studies.⁴⁷ The 40% (w/w) water mixture of $[\text{C}_5(\text{C}_{10}\text{Im})_2]\cdot 2\text{Br}$ forms a hexagonal phase from a random mixture of water and ions. A volume map of the density of polar and nonpolar regions of the mixture is shown in Figure 3. The transparent green region in the figure represents the polar groups, which includes the head groups of the cations, the anions, and the water beads. The hydrophobic region in the mixture, that is, the tail groups of the cations, is shown in magenta. We observed the hydrophobic region aggregating and forming a hexagonal lattice. This separation of polar regions occurred through the interactions of anions, head groups, and water, mediated by hydrogen bonds. In the CG model, even though the explicit hydrogen-bonded interactions are absent, they are implicitly built into the model potential. One can observe the hexagonal lattice of the hydrophobic region from the figure. The mixture was very viscous, and the formation of the perfect hexagonal phase was not complete even after a 1- μs simulation. The separation between the hydrophobic regions was computed from the structure factor to be 33 \AA .

3.3. Tail-Group Distribution. The fraction of tail groups involved in the formation of nonpolar aggregates in the 40% (w/w) aqueous mixture is shown in Figure 4a. A hydrophobic group is considered to belong to an aggregate if it is within a certain distance of any other hydrophobic group of that aggregate. The cutoff distance was chosen to be 9.5 \AA for the Bulk-I mixture. One can observe from the figure that most of the tail groups are involved in the formation of an aggregate of size 58. Figure 4b shows the distribution of tail groups for the other bulk systems studied. All of the histograms included in this figure were averaged over last 60 ns of data. The cutoff for the systems shown in Figure 4b was chosen to be 10.5 \AA . This cutoff was chosen

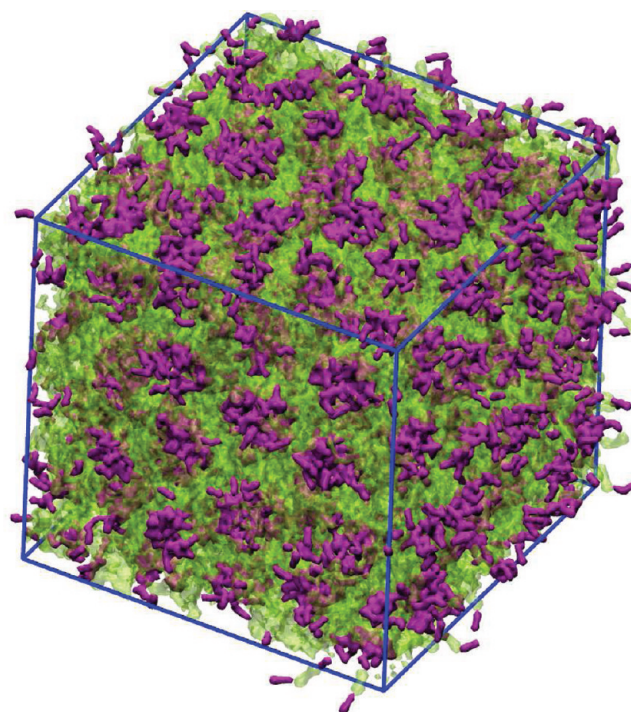


Figure 3. Volume map of the density of polar and nonpolar regions of the 40% (w/w) water mixture of $[\text{C}_5(\text{C}_{10}\text{Im})_2]\cdot 2\text{Br}$ after a 1- μs simulation. Polar regions are shown in transparent green, and nonpolar regions are shown in magenta.

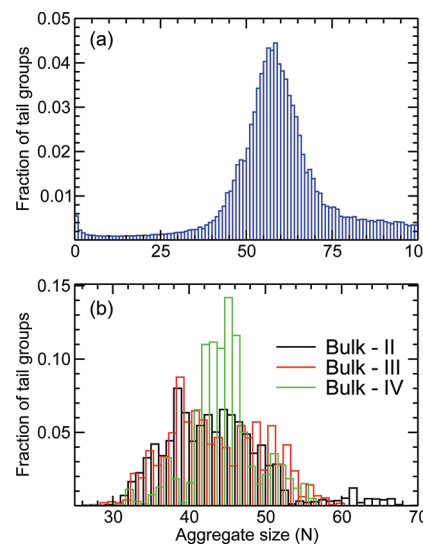


Figure 4. Fraction of tail groups involved in the formation of aggregates of size N in various water–IL systems: (a) Bulk-I and (b) Bulk-II, Bulk-III, and Bulk-IV. For visual clarity, Bulk-III and Bulk-IV are shifted by $1/3$ and $2/3$ units, respectively, along the X axis. Aggregate size (N) refers to the number of tail groups involved.

based on visual inspection of the systems. In the case of Bulk-I, because of the high concentration of the IL, a lower cutoff was used. For Bulk-III and Bulk-IV, the histograms are shifted by $1/3$ and $2/3$ units, respectively, along the X axis for the ease of visualization. It can be observed that most of the tail groups are involved in the formation of aggregates with sizes between 35 and 50. These numbers can be

compared to the experimentally observed values^{16,20} of 27–47 for the aqueous solution of $[C_{10}mim][Br]$ and also the results of computational studies⁴⁷ of $[C_{10}mim][Br]$ using coarse-grained MD simulations, which predicted values of 40–60. Experimental results are usually based on the assumption of equilibrium between monomers and monodisperse aggregates and thus yield a single value, whereas in the MD simulations, we observed a broad distribution for the aggregation numbers.

3.4. Aggregation. The aggregation of long-alkyl-chain substituted ILs in aqueous solution has been reported by several groups using various experimental methods.^{19,23} However, few of these works focused on determining the structure of the aggregates.^{2,20} In monocationic ILs with alkyl chains longer than octyl, formation of spherical aggregates has been observed using atomistic and CG-MD simulations.^{25,47} It was also found that the aggregates grow in size with the length of the alkyl chain.²⁶ Also, the shape of the aggregates was found to become more spherical and then turn into a more ordered liquid-crystalline form with increasing chain length. Neither the structure of the aggregates nor the mesophase behavior has been reported for dicationic ILs. Atomistic simulation studies of the IL $[C_3(C_{10}Im)_2] \cdot 2Br$ showed that the aggregates are interconnected by mediating cations that share their alkyl tails with different aggregates.⁴⁵ However, the size of the system and length of the atomistic simulations made it difficult to predict the level of symmetry of these interconnected aggregates. The present CG-MD simulations bridge this gap.

A snapshot of the Bulk-II system is shown in Figure 5a. In the figure, only the cations are shown. The polar (head group) and nonpolar (tail group) regions are shown in yellow and magenta, respectively. The positions of the beads were averaged over several frames. From the figure, one can see that the hydrophobic beads interact with each other favorably and are separated from the water by forming the core of the aggregates. The hydrophilic regions surround the alkyl tail groups and also interact favorably with water. The anions are mainly found near the head groups. The presence of two head groups and two tail groups in the cation imparts a distinctive structure to the aggregates compared to those of their monocationic counterparts. Aggregates are connected to each other through a mediating head group, where some cations are part of two different aggregates with each tail belonging to a unique aggregate core. Networking of micelles in gemini (dicationic) surfactants, to form threadlike and treelike structures, was also observed earlier.³⁷ Furthermore, if one considers the large-scale structure, the cores of the aggregates are located on a hexagonal lattice. The observed hexagonal structure in the system is not perfect, as not all hydrophobic cores are interconnected to six neighboring cores. The length of the simulations was likely not sufficient for the system to arrive at an equilibrated hexagonal structure. Nevertheless, the simulations provide very good detail about the mesophasic structure of the solution. The Bulk-III, Bulk-IV, and Interface simulations also yielded interconnected aggregates forming a hexagonal structure. When the solution was dilute, more regions devoid of cations were observed, but the cations still formed interlinked aggregates. The hexagonal arrangement of the hydrophobic region and a large region without ions, in the case of the Bulk-III simulations, can be observed from Figure 5b.

3.5. Aggregation Process. Snapshots of the dilute aqueous solution (Bulk-IV) at various time intervals are shown in Figure 6a–d, where the polar and nonpolar regions are depicted in yellow and magenta, respectively. Figure 6a shows the system after 1 ns, with the cations dispersed randomly throughout the

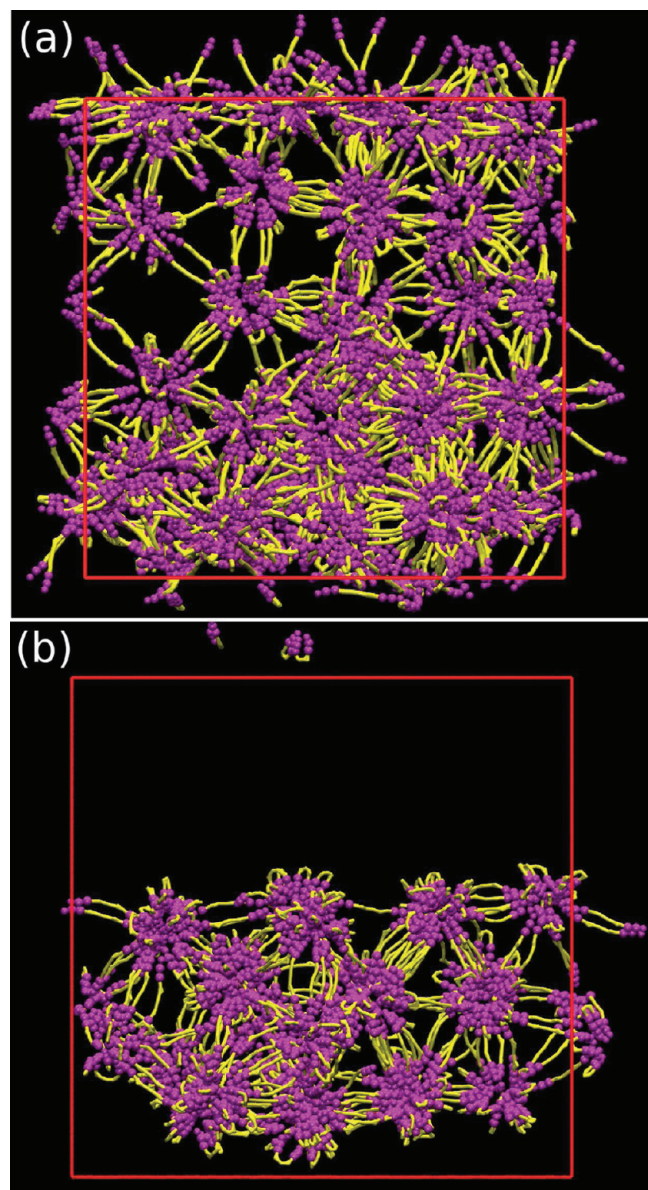


Figure 5. Snapshots of the (a) Bulk-II and (b) Bulk-III systems after a 1- μ s simulation. Polar and nonpolar regions of the cations are drawn in yellow and magenta, respectively. Anions and water beads are not shown.

solution. After several nanoseconds, small aggregate clusters are formed, some of which are loosely connected to other aggregates whereas others are not (Figure 6b, after 16 ns). These small aggregates are spherical and are dispersed in the solution. The snapshot of the system after 110 ns (Figure 6c) shows that the aggregates start moving closer to each other and are also linked to other aggregates. At this stage, most of the aggregates are connected to other aggregates and are localized to a small region of the solution. Figure 6d shows the system at the end of 1 μ s, where one can observe aggregates that are connected to one another in such a way as to form a closed structure. The hydrophobic core within this cationic aggregate shows a near-hexagonal arrangement similar to those seen in relatively concentrated solutions.

3.6. Vapor–Liquid Interface. Surface behavior is an important characteristic of aqueous solutions of amphiphilic molecules.

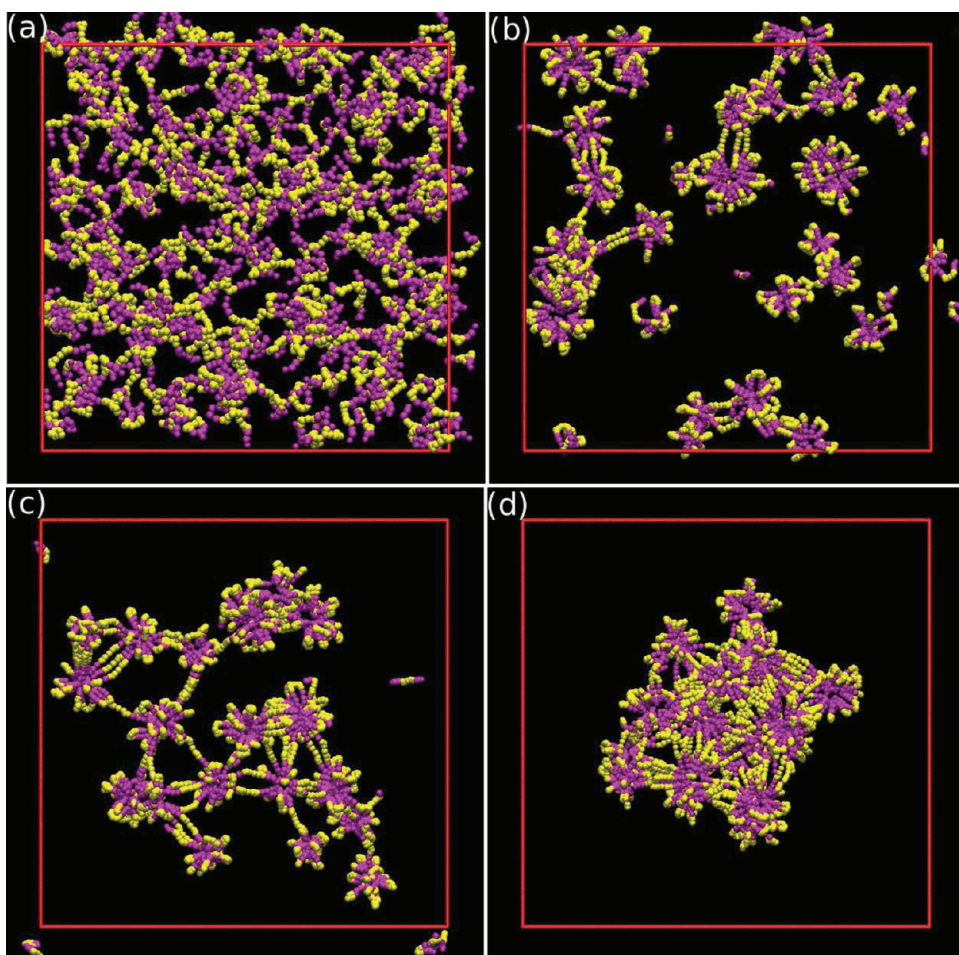


Figure 6. Snapshots of a dilute bulk system (Bulk-IV) at different stages of aggregation, after (a) 1 ns, (b) 16 ns, (c) 110 ns, and (d) 1 μ s. Polar and nonpolar groups are shown in yellow and magenta, respectively. Water and anions are not shown for ease of visualization.

The amphiphiles tend to organize at the surface so as to minimize their energy, allowing for favorable interactions and shielding unfavorable contacts. At the vapor–liquid interface of an aqueous solution, this can be achieved by protruding the tail region out of the solution and keeping the head group just below the interface. In very dilute solutions, all of the amphiphilic molecules occupy the interface. As the concentration of the solute is increased, the interface becomes saturated, and some of the molecules must remain within the solution. Beyond the CMC, these molecules tend to aggregate to form micelles.

We observed such phenomena in our studies. The average area occupied by an alkyl chain at the interface was found to be $1.03 \pm 0.01 \text{ nm}^2$, which can be compared to the experimentally reported²² minimum area per surfactant molecule for the ionic liquid $[\text{C}_{10}\text{mim}]^+[\text{Cl}]^-$ of 0.85 nm^2 . The value of 1.21 nm^2 was reported for a monocationic IL based on pyridinium cation and chloride anion with a decyl side chain.¹ The number density profiles along the interface normal (Z axis) for the rings and tail groups of the cations, the anions, and the water molecules are shown in Figure 7. The profiles were averaged over the last 60 ns of the trajectories and also over the two interfaces. $Z = 0$ refers to the center of the box along the Z axis. Ring and tail refers to the center of the imidazolium rings and the terminal bead of the alkyl chains, respectively. From the figure, one can observe that the profile for the alkyl tail shows a sharp peak at the interface and

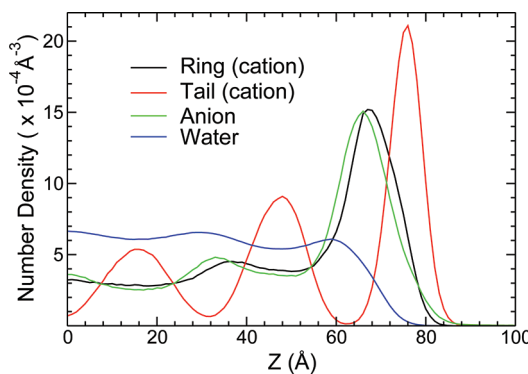


Figure 7. Number density profiles of anion, cation ring, cation tail, and water along the Z axis. The profiles are averaged over two interfaces.

also protrudes out of the interface toward the vacuum. The profile for water is normalized for comparison. The rings are located just below the interface, and anions are located closer to the cation rings. Strong peaks can also be observed in these profiles. Toward the bulk region, the profiles for the anions and imidazolium rings show a small oscillation. The number density profile of the tails shows strong oscillations well toward the center of the box. These oscillations arise from the aggregation of

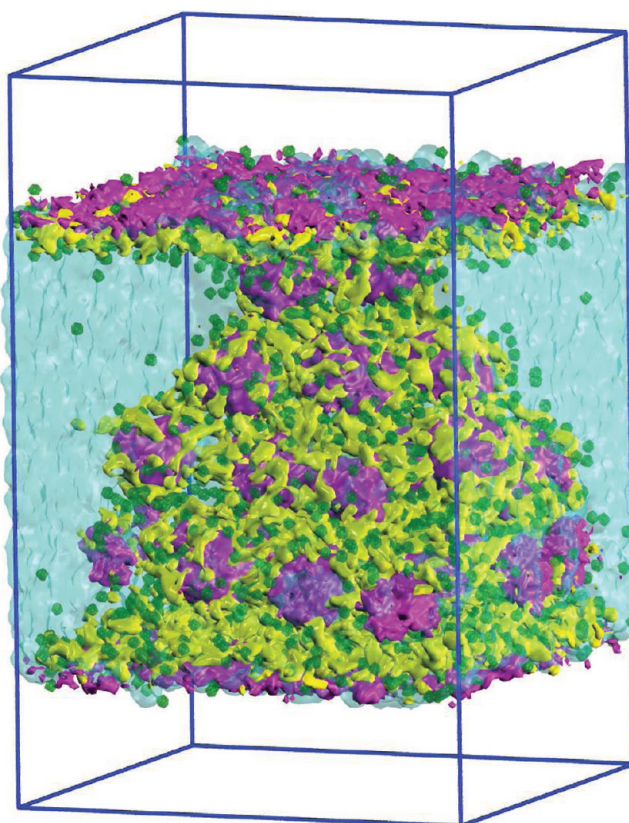


Figure 8. Volume map of the density of polar (yellow) and nonpolar (magenta) regions of the cation, anions (green), and water (cyan) at the vapor–liquid interface of the IL after 1 μ s.

the tail regions to form hydrophobic cores at a particular distance from the interface. The distance between the peaks is ~ 30 Å. One can also observe that the minima in the profile of the cationic tail are always present at the maxima for the water density profile and vice versa, which is due to the excluded volume of the hydrophobic cores of the aggregates.

The volume map of the densities of the polar (yellow) and nonpolar (magenta) regions of the cations, the anions (green), and the water molecules (cyan) is shown in Figure 8. From the figure, one can see that the interface is populated by hydrophobic groups that are aligned outward toward the vacuum. Some of the cations have both decyl tails pointing toward the vacuum, whereas a few of them have one tail at the interface and the other belonging to the aggregate within the solution. The presence of hydrophobic cores at four different layers within the solution can be observed from the figure. It is these planes that show maxima for the number density profile of the tails along the Z axis. These planes are separated ~ 30 Å from each other. The hexagonal arrangement of the hydrophobic region can also be visualized. Anions are located close to the head groups, and very few anions are found in the region that is predominantly water.

4. CONCLUSIONS

CG-MD simulations have been performed on aqueous solutions of the IL $[C_5(C_{10}Im)_2] \cdot 2Br$ at room temperature using a force field developed based on atomistic MD data. Several aqueous solutions with different concentrations of IL and a vapor–liquid interfacial system were simulated for a time of

about 1 μ s. The binary mixture of IL and water at 40% (w/w) water exhibits a hexagonal phase. The observed separation between the units is similar to that reported for the monocationic counterpart $[C_{10}mim][Br]$ at a similar concentration.¹⁴

In relatively dilute solutions, the cations form interconnected aggregates, in which the hydrophobic regions are grouped together to form a core, surrounded by the hydrophilic head groups, which are exposed to water. Whereas the majority of cations contribute both of their alkyl tails to the formation of a single aggregate, a few of them provide one alkyl tail to each of two different aggregates, with the hydrophilic region forming a bridge between the two aggregates. This peculiar interconnection, which is also seen from atomistic MD simulations,⁴⁵ is not observed in the case of monocationic ILs. The majority of hydrophobic cores were found to be composed of around 35–50 alkyl tails, leading to a broad distribution of aggregation numbers. The dilution of the solution does not affect the near hexagonal interconnection between the aggregates. Even the most dilute system studied (88 mM) shows linkage between the aggregates, with a vast region of water devoid of any ions. In the case of dilute solutions, the initial formation of small spherical aggregates dispersed throughout the solution is followed by interlinking between the aggregates, leading to a compact arrangement with all of the aggregates confined to a small region of the system.

The vapor–liquid interface of the system shows a typical behavior of amphiphilic molecules, with the hydrophobic region present at the interface protruding toward the vapor region and the hydrophilic region present just below the interface in the solution phase. Both cations and anions show an enhanced number density at the interface. Whereas the anion and the imidazolium rings exhibit small oscillations toward the bulk region of the density profile, pronounced oscillations are seen in the number density of the tail group. The spacing of the peaks, which is approximately 30 Å, corresponds to the hexagonal packing of hydrophobic cores. Anions are rarely found far from the imidazolium head groups in the solution.

The atomistic representation of the largest system studied herein would have 758000 particles. The simulation of such a large system even for a short time (10–100 ns) requires extensive computational resources and is not currently feasible. The mesophasic structures of viscous systems such as the $[C_5(C_{10}Im)_2] \cdot 2Br$ –water mixture or the equilibrium structure of micellar aggregates of aqueous solutions of $[C_5(C_{10}Im)_2] \cdot 2Br$ are nearly impossible to simulate using atomistic MD simulations. In addition, the soft potentials used in the coarse-grained force field accelerate the dynamics of the system. Even though some details such as explicit hydrogen bonding are lost, CG-MD simulations provide valuable insights into the structure and slow processes of viscous systems. Atomistic MD simulations are valuable in developing CG force fields.

The present studies were carried out on solutions at concentrations that are higher than the CMC. The structure of aggregates near the CMC might be different from that observed in these studies. Also, it will be interesting to examine the structure of the solution near the CMC and to study whether there is a critical concentration below which the aggregates are dispersed randomly.

■ AUTHOR INFORMATION

Corresponding Author

*Phone: +1-215-204-4217. Fax: +1-215-204-2257. E-mail: bhargav@sas.upenn.edu.

■ ACKNOWLEDGMENT

We are grateful for the support from the College of Science and Technology at Temple University and the Ras Al Khaimah Center for Advanced Materials for a research fellowship named for His Highness Sheikh Saqr Bin Mohammed Al Qasimi. Some of the simulations were performed using teragrid resources.

■ REFERENCES

- (1) Blesic, M.; Lopes, A.; Melo, E.; Petrovski, Z.; Plechkova, N. V.; Lopes, J. N. C.; Seddon, K. R.; Rebelo, L. P. N. *J. Phys. Chem. B* **2008**, *112*, 8645–8650.
- (2) Bowers, J.; Butts, C. P.; Martin, P. J.; Vergara-Gutierrez, M. C. *Langmuir* **2004**, *20*, 2191–2198.
- (3) Miskolczy, Z.; Sebök-Nagy, K.; Biczók, L.; Göktürk, S. *Chem. Phys. Lett.* **2004**, *400*, 296–300.
- (4) Luczak, J.; Hupka, J.; Thöming, J.; Jungnickel, C. *Colloids Surf. A* **2008**, *329*, 125–133.
- (5) Bhargava, B. L.; Yasaka, Y.; Klein, M. L. *Chem. Commun.* **2011**, *47*, 6228–6241.
- (6) Triolo, A.; Mandanici, A.; Russina, O.; Rodriguez-Mora, V.; Cutroni, M.; Hardacre, C.; Nieuwenhuyzen, M.; Bleif, H.; Keller, L.; Ramos, M. A. *J. Phys. Chem. B* **2006**, *110*, 21357–21364.
- (7) Triolo, A.; Russina, O.; Bleif, H.; Di Cola, E. *J. Phys. Chem. B* **2007**, *111*, 4641–4644.
- (8) Xiao, D.; Rajian, J. R.; Li, S.; Bartsch, R. A.; Quitevis, E. L. *J. Phys. Chem. B* **2006**, *110*, 16174–16178. Xiao, D.; Rajian, J. R.; Cady, A.; Li, S.; Bartsch, R. A.; Quitevis, E. L. *J. Phys. Chem. B* **2007**, *111*, 4669–4677.
- (9) Hu, Z.; Margulis, C. *J. Acc. Chem. Res.* **2007**, *40*, 1097–1105.
- (10) Maginn, E. *J. J. Phys.: Condens. Matter* **2009**, *21*, 373101.
- (11) Annapureddy, H. V. R.; Hu, Z.; Xia, J.; Margulis, C. *J. Phys. Chem. B* **2008**, *112*, 1770–1776.
- (12) Shi, W.; Maginn, E. *J. Phys. Chem. B* **2008**, *112*, 2045–2055.
- (13) Firestone, M. A.; Dzielawa, J. A.; Zapol, P.; Curtiss, L. A.; Seifert, S.; Dietz, M. L. *Langmuir* **2002**, *18*, 7258–7260.
- (14) Firestone, M. A.; Rickert, P. G.; Seifert, S.; Dietz, M. L. *Inorg. Chim. Acta* **2004**, *357*, 3991–3998.
- (15) Inoue, T.; Dong, B.; Zheng, L. *J. Colloid Interface Sci.* **2007**, *307*, 578–581.
- (16) Goodchild, I.; Collier, L.; Millar, S. L.; Prokes, I.; Lord, J. C. D.; Butts, C. P.; Bowers, J.; Webster, J. R. P.; Heenan, R. K. *J. Colloid Interface Sci.* **2007**, *307*, 455–468.
- (17) Hanke, C. G.; Atamas, N. A.; Lynden-Bell, R. M. *Green Chem.* **2002**, *4*, 107–111.
- (18) Lynden-Bell, R. M. *Mol. Phys.* **2003**, *101*, 2625–2633.
- (19) Blesic, M.; Marques, M. H.; Plechkova, N. V.; Seddon, K. R.; Rebelo, L. P. N.; Lopes, A. *Green Chem.* **2007**, *9*, 481–490.
- (20) Zhao, Y.; Gao, S.; Wang, J.; Tang, J. *J. Phys. Chem. B* **2008**, *112*, 2031–2039.
- (21) Bhargava, B. L.; Klein, M. L. *Soft Matter* **2009**, *5*, 3475–3480.
- (22) El Seoud, O. A.; Pires, P. A. R.; Abdel-Moghny, T.; Baston, E. L. *J. Colloid Interface Sci.* **2007**, *313*, 296–304.
- (23) Vanyur, R.; Biczók, L.; Miskolczy, Z. *Colloids Surf. A* **2007**, *299*, 256–261.
- (24) Jiang, W.; Wang, Y.; Voth, G. A. *J. Phys. Chem. B* **2007**, *111*, 4812–4818.
- (25) Bhargava, B. L.; Klein, M. L. *J. Phys. Chem. A* **2009**, *113*, 1898–1904.
- (26) Bhargava, B. L.; Klein, M. L. *J. Phys. Chem. B* **2009**, *113*, 9499–9505.
- (27) Feng, S.; Voth, G. A. *Fluid Phase Equilib.* **2010**, *294*, 148–156.
- (28) Anderson, J. L.; Ding, R.; Ellern, A.; Armstrong, D. W. *J. Am. Chem. Soc.* **2005**, *127*, 593–604.
- (29) Baltazar, Q. Q.; Chandawalla, J.; Sawyer, K.; Anderson, J. L. *Colloids Surf. A* **2007**, *302*, 150–156.
- (30) Ding, Y.; Zha, M.; Zhang, J.; Wang, S. *Colloids Surf. A* **2007**, *298*, 201–205.
- (31) Lovelock, K. R. J.; Deyko, A.; Corfield, J.-A.; Gooden, P. N.; Licence, P.; Jones, R. G. *ChemPhysChem* **2009**, *10*, 337–340.
- (32) Liu, X.; Xiao, L.; Wu, H.; Chen, J.; Xia, C. *Helv. Chim. Acta* **2009**, *92*, 1014–1021.
- (33) Chang, J.; Ho, W.; Sun, I.; Tung, Y.; Tsui, M.; Wu, T.; Liang, S. *Tetrahedron* **2010**, *66*, 6150–6155.
- (34) Han, X.; Armstrong, D. W. *Org. Lett.* **2005**, *7*, 4205–4208.
- (35) Liu, Q.; van Rantwijk, F.; Sheldon, R. A. *J. Chem. Technol. Biotechnol.* **2006**, *81*, 401–405.
- (36) Fang, D.; Yang, J.; Ni, C. *Heteroatom Chem.* **2011**, *22*, 5–10.
- (37) Karaborni, S.; Esselink, K.; Hilbers, P. A. J.; Smit, B.; Karthauser, J.; van Os, N. M.; Zana, R. *Science* **1994**, *266*, 254–256.
- (38) Kern, F.; Lequeux, F.; Zana, R.; Candau, R. J. *Langmuir* **1994**, *10*, 1714–1723.
- (39) Karaborni, S.; Smit, B. *Curr. Opin. Colloid Interface Sci.* **1996**, *1*, 411–415.
- (40) Jin, C.; Ye, C.; Phillips, B. S.; Zabinski, J. S.; Liu, X.; Liu, W.; Shreeve, J. M. *J. Mater. Chem.* **2006**, *16*, 1529–1535.
- (41) Han, X.; Armstrong, D. W. *Acc. Chem. Res.* **2007**, *40*, 1079–1086.
- (42) Nachtigall, F. M.; Corilo, Y. E.; Cassol, C. C.; Ebeling, G.; Morgan, N. H.; Dupont, J.; Eberlin, M. N. *Angew. Chem., Int. Ed.* **2008**, *47*, 151–154.
- (43) Sun, H.; Zhang, D.; Liu, C.; Zhang, C. *J. Mol. Struct. (THEOCHEM)* **2009**, *900*, 37–43.
- (44) Nooruddin, N. S.; Wahlbeck, P. G.; Carper, W. R. *Tribol. Lett.* **2009**, *36*, 147–156.
- (45) Bhargava, B. L.; Klein, M. L. *J. Chem. Theory Comput.* **2010**, *6*, 873–879.
- (46) Bhargava, B. L.; DeVane, R.; Klein, M. L.; Balasubramanian, S. *Soft Matter* **2007**, *3*, 1395–1400.
- (47) Bhargava, B. L.; Klein, M. L. *Mol. Phys.* **2009**, *107*, 393–401.
- (48) Shinoda, W.; DeVane, R.; Klein, M. L. *Mol. Simul.* **2007**, *33*, 27–36.
- (49) Plimpton, S. *J. Comput. Phys.* **1995**, *117*, 1–19.
- (50) Tuckerman, M. E.; Berne, B. J.; Martyna, G. J. *J. Chem. Phys.* **1992**, *97*, 1990–2001.
- (51) Humphrey, W.; Dalke, A.; Schulten, K. *J. Mol. Graphics* **1996**, *14*, 33–38.